Large-scale flow in turbulent convection: a mathematical model

By L. N. HOWARD

Department of Mathematics, Florida State University, Tallahassee, Florida 32306, USA

AND R. KRISHNAMURTI

Department of Oceanography, Florida State University, Tallahasse, Florida 32306, USA

A mathematical model of convection, obtained by truncation from the two-dimensional Boussinesq equations, is shown to exhibit a bifurcation from symmetrical cells to tilted non-symmetrical ones. A subsequent bifurcation leads to time-dependent flow with similarly tilted transient plumes and a large-scale Lagrangian mean flow. This change of symmetry is similar to that occurring with the advent of a large-scale flow and transient tilted plumes seen in laboratory experiments on turbulent convection at high Rayleigh number. Though not intended as a description of turbulent convection, the model does bring out in a theoretically tractable context the *possibility* of the spontaneous change of symmetry suggested by the experiments.

Further bifurcations of the model lead to stable chaotic phenomena as well. These are numerically found to occur in association with heteroclinic orbits. Some mathematical results clarifying this association are also presented.

1. Introduction and summary

In a horizontal layer of fluid with fixed higher temperature on the bottom boundary and fixed lower temperature on the top boundary, cellular convective flow occurs for a certain range of Rayleigh number R and Prandtl number σ. The horizontal scale of these cells is comparable with the depth of the layer. At successively larger values of R, a number of transitions in the flow pattern as well as in the heat flux are observed (Malkus 1954; Willis & Deardorff 1967a, b; Krishnamurti 1970a, b; Busse & Whitehead 1971). Most of these changes are within the regime of cellular flows. Recent laboratory studies (Krishnamurti & Howard 1981) showed a further transition which leads to a very different scale of motion and very different transport properties. At $\sigma = 7$ and $R = 10^6$, the flow consists of transient plumes or bubbles of hot fluid rising from the bottom boundary and cold ones sinking from the top boundary. (x, t)-photographs (where x is a horizontal coordinate, t is the time) of the flow revealed that there is nothing that could be identified as a cell boundary, unlike the case at lower R and/or higher σ. When R was made greater than approximately 2×10^6, these plumes began to drift in one direction along the bottom layer, and in the opposite direction near the top of the layer. Thus the flow in this regime has apparently two distinct scales of motion. The smaller-scale flow (the transient plumes or bubbles) has a horizontal lengthscale comparable with the layer depth d, while the large-scale flow (the apparent horizontal drift which is oppositely directed near the bottom and the top of the layer) has a lengthscale that is the layer width L. In those experiments L was typically an

order of magnitude larger than d. In further experiments the fluid occupied a cylindrical annular region and the plumes were observed to drift all in one direction along the bottom, and all in the opposite direction along the top.

When this apparent large-scale flow occurred, we observed that nearly all these plumes were uniformly tilted away from the vertical in such a way that the momentum transport by the Reynolds stress $\overline{uw}$ would tend to maintain this large-scale flow. Here u is the horizontal velocity, w the vertical velocity. The large-scale horizontal velocity $\bar{u}(z)$ was inferred from the apparent speed of horizontal motion of the plumes. These plumes were visualized by means of tracers which show regions of change of shear in the fluid velocity. Thus from the observed movement of the location of strong shear zones, one could not conclude that mass was moving with the same velocity. In experiments to be described in a forthcoming paper, the actual velocity of neutrally buoyant microscopic tracer particles in a cylindrical annulus of turbulent convecting fluid was measured and the existence of an Eulerian velocity $\bar{u}(z)$, non-zero after horizontal average around the annulus, was demonstrated. Furthermore, by the introduction of dyed fluid, we observed that there was a net horizontal Lagrangian velocity also. From these velocity measurements we found that the Reynolds-stress divergence very nearly balances the viscous force on the large-scale flow $\bar{u}(z)$. The main results of this experiment are: (i) There does exist a non-zero horizontally averaged velocity $\bar{u}(z)$, correctly inferred by the apparent drift of the plumes. (ii) The direction of momentum transport by the Reynolds stress is up the gradient of $\bar{u}$. The Reynolds stress balances the viscous force on the large-scale flow.

With the onset of this large-scale horizontal flow, the largest scale of motion has increased from one comparable with the layer depth to one comparable with the layer width. The onset has the semblance of an instability; it seems to set in at a certain Rayleigh number, and there is associated with it a change in the symmetry of the flow.

In §2 a mathematical model of this flow is presented. It was proposed in order to test the possibility that a large-scale shearing flow might occur as a result of an instability of cellular flow. To this end the three Fourier components that lead to the Lorenz equations (Lorenz 1963) were augmented with three additional components, leading to a sixth-order system. The main results of a study of the bifurcations of the resulting sixth-order system are that:

(i) After the second bifurcation, steady tilted cells are the stable flow. This symmetry change is like that observed in the laboratory. While steady tilted cells are not observed in a convecting layer of fluid, they have been seen in Hele-Shaw cell convection.

(ii) After the third bifurcation, stable limit cycles are found for a range of R and σ with the same symmetry as in (i). The flow and thermal structure can be described as hot transient plumes that form periodically and tilt as they rise from below, and cold ones that sink from above with the same angle of tilt. In this range, there is a net Lagrangian transport of mass, in one horizontal direction near the top of the layer, and in the opposite direction near the bottom. Although this very limited two-dimensional model cannot at all simulate the experiments, nevertheless the tilting transient plumes and the Lagrangian transport are qualitatively similar to the laboratoi · observations.

(iii) Within this range of R where stable limit cycles are found, there are narrow sub-ranges of aperiodic flows. The occurrence of this chaotic behaviour is shown to be related to the existence of heteroclinic orbit pairs.

2. The mathematical model

By truncating a Fourier representation of the stream function and temperature field, we obtain a set of equations governing the amplitudes of the Fourier modes. The three components that give rise to the Lorenz equations have here been augmented by three more, in particular so that in the stream function one mode is included that is independent of the horizontal coordinate x. Such a mode has not been included in previous studies (e.g. Curry 1978); without the observation that a large-scale flow can occur, there would be little reason to do so. The bifurcations of the resulting sixth-order system are studied. The main purpose was to see if, in such a simplified but manageable system, a large-scale circulation could arise spontaneously as an instability on cellular convection. The relationship between the bifurcations of the truncated model equations and of the Boussinesq equations is yet to be established.

The dimensionless vorticity equation and the heat equation, in the Boussinesq approximation, are

$$\frac{\partial}{\partial t} \nabla^2 \Psi = \sigma \nabla^4 \Psi + \sigma \frac{\partial \Theta}{\partial x} + \frac{\partial(\Psi, \nabla^2 \Psi)}{\partial(x, z)}, \tag{1}$$

$$\frac{\partial \Theta}{\partial t} = \nabla^2 \Theta + R \frac{\partial \Psi}{\partial x} + \frac{\partial(\Psi, \Theta)}{\partial(x, z)} \tag{2}$$

where Ψ is the stream function, $\partial \Psi / \partial x = -w$, $\partial \Psi / \partial z = u$, and Θ is the negative temperature perturbation. The Rayleigh number R and the Prandtl number σ are defined by

$$R = \frac{g\alpha}{\kappa\nu} \Delta T d^3, \quad \sigma = \frac{\nu}{\kappa},$$

where g is the acceleration due to gravity, α the thermal expansion coefficient, κ the thermal diffusivity, ν the kinematic viscosity, πd the layer depth, and ΔT the imposed temperature difference between the bottom and top boundaries of the layer. These equations together with the boundary conditions $\Theta = \Psi = \nabla^2 \Psi = 0$ on $z = 0, \pi$ are invariant under x-translations. The only solutions also invariant under all such translations (i.e. independent of x) satisfy

$$\frac{\partial}{\partial t} \Psi_{zz} = \sigma \frac{\partial^4 \Psi}{\partial z^4}, \quad \frac{\partial \Theta}{\partial t} = \Theta_{zz}$$

which, with the boundary conditions, imply that Θ and $\Psi \to 0$ as $t \to \infty$. Any instability of the basic state of conduction must thus involve the breaking of the symmetry implied by invariance under x-translations. One may reasonably expect that most solutions of interest will nevertheless be invariant under some discrete subgroup of the translations, and in accordance with tradition we shall consider only solutions which are periodic in x with wavenumber α, i.e. invariant under translations through $2\pi/\alpha$. Such solutions will be represented, with regard to their x-dependence, by Fourier series in $\sin n\alpha x$ and $\cos n\alpha x$. Because of the structure of the equations and boundary conditions it is also convenient to represent the z-dependence of Θ and Ψ by Fourier sine series; in view of the boundary conditions at $z = 0$ and π the Fourier series of z-derivatives up to the fourth are correctly given by formal term-by-term differentiation of the series.

Now the equations and boundary conditions are also invariant under the transformation

$$R: z \to \pi - z, \quad \Theta \to -\Theta, \quad \Psi \to -\Psi,$$

i.e. reflection in the mid-plane $z = \frac{1}{2}\pi$ and reversal of temperatures and vertical (but not horizontal) velocities; and they are invariant under

$$\text{T}: x \rightarrow x + \pi/\alpha,$$

an x-translation by half a wavelength. Some, but not all, of the x-periodic solutions are invariant under the composition TR (= RT) of these. For example the steady cellular convection which sets in at the critical Rayleigh number has alternating clockwise and counterclockwise rotating cells, with hot rising and cold descending regions – with a suitable choice of x-origin they are represented fairly well by functions of the form

$$\Psi = A \sin \alpha x \sin z, \\ \Theta = D \cos \alpha x \sin z + E \sin 2z. \tag{3}$$

The transformation R reverses the direction of rotation of the cells and interchanges hot and cold perturbations but since the cells are symmetrical, following R by T restores the original situation. Because the infinitesimal solution at the critical Rayleigh number possesses this RT symmetry it is natural to restrict attention to such solutions in studying finite-amplitude cellular convection (in two dimensions), and this is normally done. This symmetry is also assumed in the truncation which leads to the Lorenz model – it uses just those terms written in (3). However the kind of large-scale flow with which we are concerned in this paper does not possess this RT invariance. We shall present a model, based on free–free two-dimensional convection and so analogous to the Lorenz model, which will illustrate the possibility of spontaneous breaking of the RT symmetry. Such a model must not of course have this symmetry built in from the start, and the form we shall use is

$$\Psi = A \sin \alpha x \sin z + B \sin z + C \cos \alpha x \sin 2z, \\ \Theta = D \cos \alpha x \sin z + E \sin 2z + F \sin \alpha x \sin 2z. \tag{4}$$

Note that the effect of RT on this is to reverse the signs of B, C and F but not those of the 'Lorenz variables' A, D and E. The effect of R alone is to reverse the signs of A, B and D and not C, E and F. Those functions of the form (4) which are invariant under RT are exactly those with $B = C = F = 0$.

The form (4) appears to be the simplest that makes some sense as a truncation of the Boussinesq equations and allows the possibility for breaking the RT symmetry. The B-term allows the possibility of a 'large-scale flow' – a horizontal shear flow independent of x. If both A and B are present, their interaction through the Jacobian in the vorticity equation requires the presence of the C-term, and it in turn requires through the temperature equation that F be present. Of course the Boussinesq equations do not really have solutions with only the terms in (4). All sorts of higher harmonics would be generated too, and our truncated model is open to the usual doubts about the relevance of such truncations to the partial differential equations they purport to 'solve'. This model does however accurately reflect some important symmetry properties of the Boussinesq equations (1) and (2). Certainly not all of their solutions have the RT symmetry though there is an 'invariant submanifold' of them that do. Whether or not (at sufficiently high R) there are attractors off this manifold, as does indeed happen in the model, we unfortunately do not know.

Substituting (4) into (2) and (3) and truncating leads to the following set of equations governing the time evolution of the coefficients A, B, C, D, E, F:

$$\dot{A} + \sigma(1 + \alpha^2)A - \frac{\sigma\alpha}{(1 + \alpha^2)}D - \frac{1}{2}\alpha\frac{(3 + \alpha^2)}{(1 + \alpha^2)}BC = 0, \tag{5}$$

$$\dot{B} + \sigma B + \tfrac{3}{4}\,\alpha AC = 0, \tag{6}$$

$$\dot{C} + \sigma(4+\alpha^2)\,C + \frac{\alpha\sigma}{(4+\alpha^2)}\,F + \frac{\alpha^3}{2(4+\alpha^2)}\,AB = 0, \tag{7}$$

$$\dot{D} + (1+\alpha^2)\,D - R\alpha A + \alpha AE + \tfrac{1}{2}\alpha\,BF = 0, \tag{8}$$

$$\dot{E} + 4E - \tfrac{1}{2}\alpha\,AD = 0, \tag{9}$$

$$\dot{F} + (4+\alpha^2)\,F + R\alpha C - \tfrac{1}{2}\alpha\,BD = 0. \tag{10}$$

Some features of these equations are:

(i) The Lorenz model, consisting of the three components with coefficients A, D, E is recovered when we set $B = C = F = 0$ in these equations.

(ii) If $R < R_{c2}$ (defined below), all trajectories in the phase space starting at points outside a certain finite region eventually enter and remain in this region so that the coordinates of the phase point are bounded as $t \to \infty$.

$R_{c2} \equiv (4+\alpha^2)^3/\alpha^2$ is the critical Rayleigh number for instability of the conduction state to the second vertical mode. Equations (5)–(10) are readily seen to have $A = B = D = E = 0$ as an invariant manifold, on which the equations in C and F are exactly linear, and unstable for $R > R_{c2}$. Thus there *are* trajectories going to infinity in this case. This is no doubt an artifact of the truncation – if only C and F are present, the model is linearly like the Lorenz model for the half-height, but does not contain the $\sin(4z)$ term in the temperature field which would nonlinearly be needed. For $R < R_{c2}$ the boundedness of trajectories as $t \to \infty$ can be demonstrated by showing that the quantity

$$Q = \frac{R}{\sigma}\,[\tfrac{1}{2}(1+\alpha^2)\,A^2 + B^2 + \tfrac{1}{2}(4+\alpha^2)\,C^2] + \tfrac{1}{2}D^2 + (E-2R)^2 + \tfrac{1}{2}F^2$$

is always decreasing when it is large. From (5)–(10) one finds that

$$\frac{dQ}{dt} = -R[(1+\alpha^2)^2 A^2 + 2B^2] - (1+\alpha^2)\,D^2 - 4(E-2R)^2$$

$$-4E^2 + 16R^2 - (4+\alpha^2)\left(1 - \left(\frac{R}{R_{c2}}\right)^{\frac{1}{2}}\right)$$

$$\times (R(4+\alpha^2)\,C^2 + F^2) - \frac{1}{4+\alpha^2}\left[R\alpha\left(\frac{R_{c2}}{R}\right)^{\frac{1}{4}} C + (4+\alpha^2)\left(\frac{R}{R_{c2}}\right)^{\frac{1}{4}} F\right]^2$$

$$\leqslant -2\,\mathrm{Min}\,\{\alpha, 1\}\,\mathrm{Min}\left\{(4+\alpha^2)\left(1 - \left(\frac{R}{R_{c2}}\right)^{\frac{1}{2}}\right), 1\right\} Q + 16\,R^2,$$

so Q is decreasing if it exceeds $8R^2/(\mathrm{Min}\,\{\alpha, 1\}\,\mathrm{Min}\,\{(4+\alpha^2)\,(1 - (R/R_{c2})^{\frac{1}{2}}), 1\})$. In this paper we shall be concerned only with $R < R_{c2}$. The minimum value of R_{c2} is 108, and it occurs at $\alpha^2 = 2$.

(iii) Since the divergence of the velocity in phase space is

$$\frac{\partial\dot{A}}{\partial A} + \frac{\partial\dot{B}}{\partial B} + \frac{\partial\dot{C}}{\partial C} + \frac{\partial\dot{D}}{\partial D} + \frac{\partial\dot{E}}{\partial E} + \frac{\partial\dot{F}}{\partial F} = -2\sigma(3+\alpha^2) - (9+2\alpha^2),$$

the density of phase points increases according to

$$\frac{1}{\rho}\frac{d\rho}{dt} = 2\sigma(3+\alpha^2) + (9+2\alpha^2)$$

(which is equal to 19 for $\sigma = 1$, $\alpha = 1$).

2.1. *Critical points and attractors*

The overall picture with respect to critical points and attractors, for different ranges of R, is indicated schematically in figure 1. In this figure, two components A and C are plotted against R. The curves of critical points are indicated by heavy solid lines where they are attracting, and by broken lines otherwise.

$0 < R \leqslant R_c$

The conduction state 0, with $A = B = C = D = E = F = 0$ is a global attractor, as with the Boussinesq equations, below the critical Rayleigh number $R_c = (1+\alpha^2)^3/\alpha^2$. All six eigenvalues of the linearization about the origin are real and negative up to $R = R_c$, where one real eigenvalue passes through zero.

$R_c < R \leqslant R^*$

Steady symmetric cells (invariant under RT transformation) are stable in this range. There are two solutions with $B = C = F = 0$ and

$$A = \pm \frac{2\sqrt{2}}{1+\alpha^2}(R-R_c)^{\frac{1}{2}},$$

$$D = \pm \frac{2\sqrt{2}\,(1+\alpha^2)}{\alpha}(R-R_c)^{\frac{1}{2}},$$

$$E = R - R_c.$$

These are labelled $L+$ and $L-$ since they lie in the Lorenz manifold, $B = C = F = 0$. In figure 1 they are shown to lie in the (A, R)-plane. The two branches correspond to the two possible directions of circulation within a cell. The linearization about $L+$ (or $L-$) leads to an eigenvalue problem that factors into two parts. One is in the Lorenz coordinates, the other in the coordinates B, C, F. In the Lorenz coordinates, linear instability never occurs if $\sigma < 1+4/(1+\alpha^2)$. For example, for $\alpha = 1.2$, the Lorenz solution in three dimensions is stable for $\sigma < 2.639$. For $\sigma > 1+4/(1+\alpha^2)$ a Hopf bifurcation occurs at $R/R_c = R_E/R_c = \sigma(\sigma+b+3)/(\sigma-b-1)$, where $b = 4/(1+\alpha^2)$, with linear oscillatory instability of $L+$ above this R. The other factor has a real eigenvalue crossing through the origin as R increases through R^*, where

$$\frac{R^*}{R_c} = \frac{\sigma^2 \dfrac{(4+\alpha^2)^3}{(1+\alpha^2)^3} + 3\sigma + 3\dfrac{\alpha^2\,(4+\alpha^2)}{(1+\alpha^2)^2}}{\sigma^2 + 3\sigma + 3\dfrac{\alpha^2\,(4+\alpha^2)}{(1+\alpha^2)^2}}.$$

This instability at R^*, which leads out of the 'Lorenz manifold' $B = C = F = 0$, occurs *first* if $\alpha > 0.5857$ ($b < 2.978$) no matter what σ may be. The Hopf bifurcation occurs below R^* only if $\alpha < 0.5857$, and then only for a limited range of values of σ (see figure 2c). Table 1 and figure 2 (a, b) and 3 show critical values for other α and σ. The stationary bifurcation at $R = R^*$ is supercritical (unlike the typical case for the Hopf bifurcation at R_E).

$R^* < R \leqslant \tilde{R}$

Steady tilted cells (not invariant under RT transformation) are stable in this range. To determine the tilted-cell critical points it is necessary to solve the six quadratic equations obtained by setting $\dot{A} = \ldots = \dot{F} = 0$ in (5)–(10). Among the solutions are of course the other critical points $L+$, $L-$ and 0. In fact it is easy to show from these equations that if $A = 0$ then all the other variables must be zero
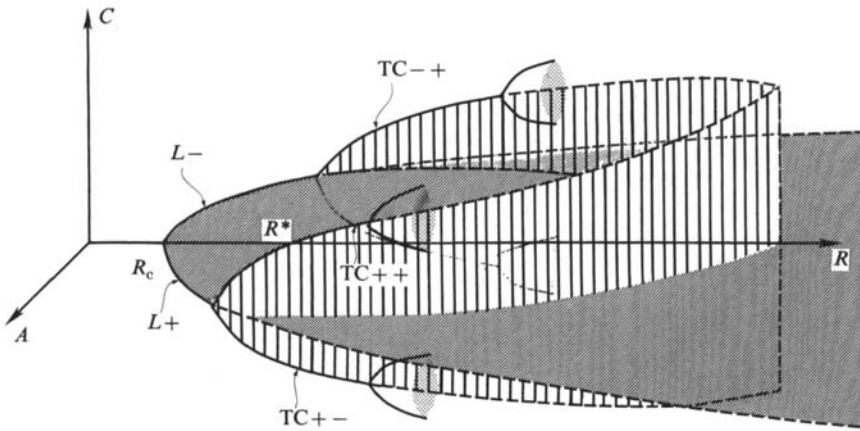
FIGURE 1. Bifurcation diagram. The amplitudes A and C vs. Rayleigh number R.

R_c	$\sigma = 0.1$	$\sigma = 1.0$	$\sigma = 10.0$
R	10.08804	10.08804	10.08804
R^*	10.32695	22.88606	86.02088
$\tilde{R}$	11.215	38.802	89.179

TABLE 1. Critical Rayleigh numbers for the onset of steady convection R_c, for the onset of steady tilted-cell convection R^*, and for the onset of oscillatory convection $\tilde{R}$. All are for $\alpha = 1.2$.

too, *unless* $R = R_{c2} = (4+\alpha^2)^3/\alpha^2$. At this special value of R (the second-mode linear instability of the origin, which is still retained by the present truncation though its nonlinear extension is inadequately represented) there is a line of critical points which may be parameterized by C, and is given by $F = -[(4+\alpha^2)^2/\alpha]\ C$ with $A = B = D = E = 0$. These occur *only* at R_2, and will not be considered further, though their analogues in a higher truncation might well be of significance. If $A \neq 0$ but $C = 0$ it is easily seen that $B = F = 0$, and we get the family of steady symmetrical cells given above as $L+$ and $L-$ in terms of R. They may also conveniently be parameterized by A in the form

$$D = \frac{(1+\alpha^2)^2}{\alpha}\,A,$$

$$E = \tfrac{1}{8}(1+\alpha^2)^2\,A^2,$$

$$R = R_c + \tfrac{1}{8}(1+\alpha^2)^2\,A^2.$$

the two signs of A for a given A^2 giving $L+$ and $L-$ for the common value of R. Finally if both A and C are not zero, one can show from (6), (5), (9) and (7) that B, D, E and F must be given in terms of A and C by

$$B = -\frac{3\alpha}{4\sigma}\,AC,$$

$$D = \frac{(1+a^2)^2}{\alpha}\,A + \frac{3\alpha(3+\alpha^2)}{8\sigma^2}\,AC^2,$$

$$E = \tfrac{1}{8}A^2\left[(1+\alpha^2)^2 + \frac{3\alpha^2(3+\alpha^2)}{8\sigma^2}\,C^2\right],$$

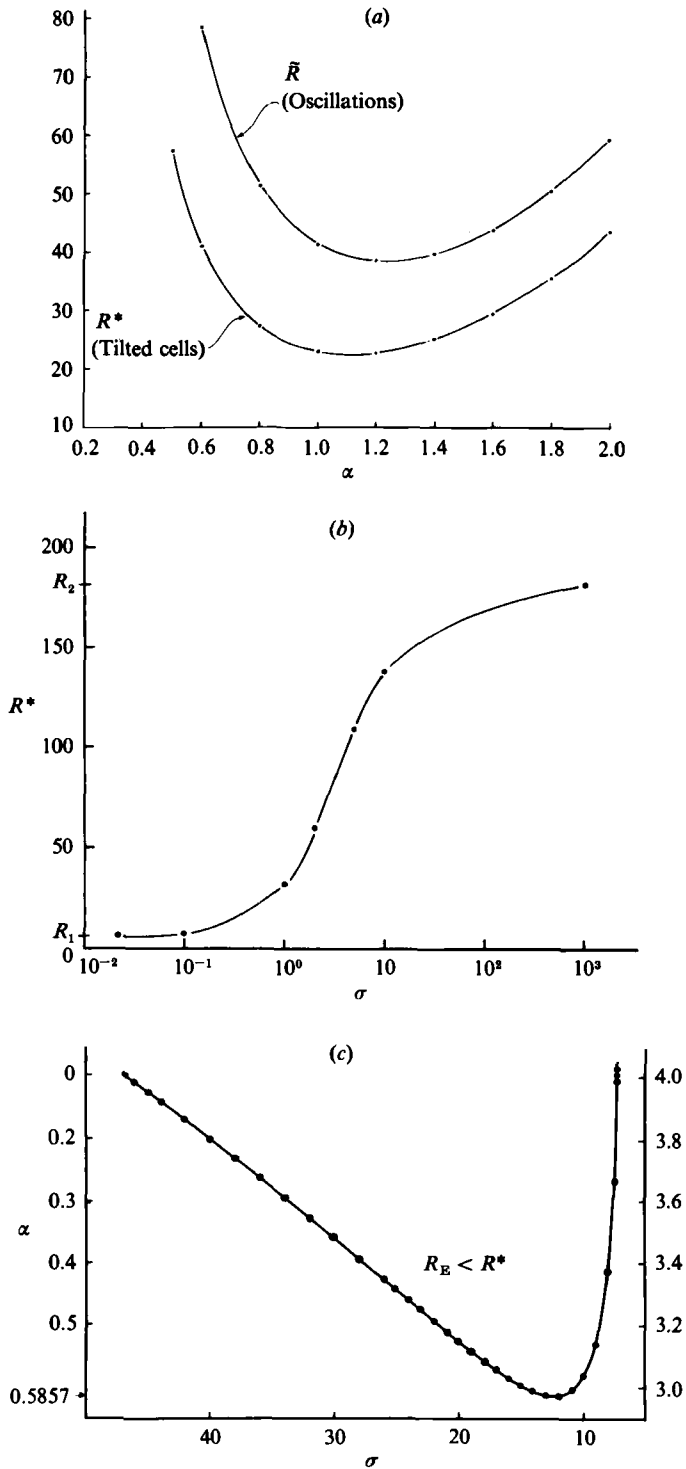$$F = \frac{-(4+\alpha^2)^2}{\alpha}\,C + \frac{3\alpha^3}{8\sigma^2}\,A^2C.$$

FIGURE 2. (a) Marginal stability diagram for onset of steady tilted cells, and oscillatory flow at $\sigma = 1.0$. (b) The critical Rayleigh number R^* for onset of tilted cells as it varies with Prandtl number σ. (c) Conditions on σ and α such that the tilted-cell instability occurs at lower R than the Hopf bifurcation of the Lorenz critical point.
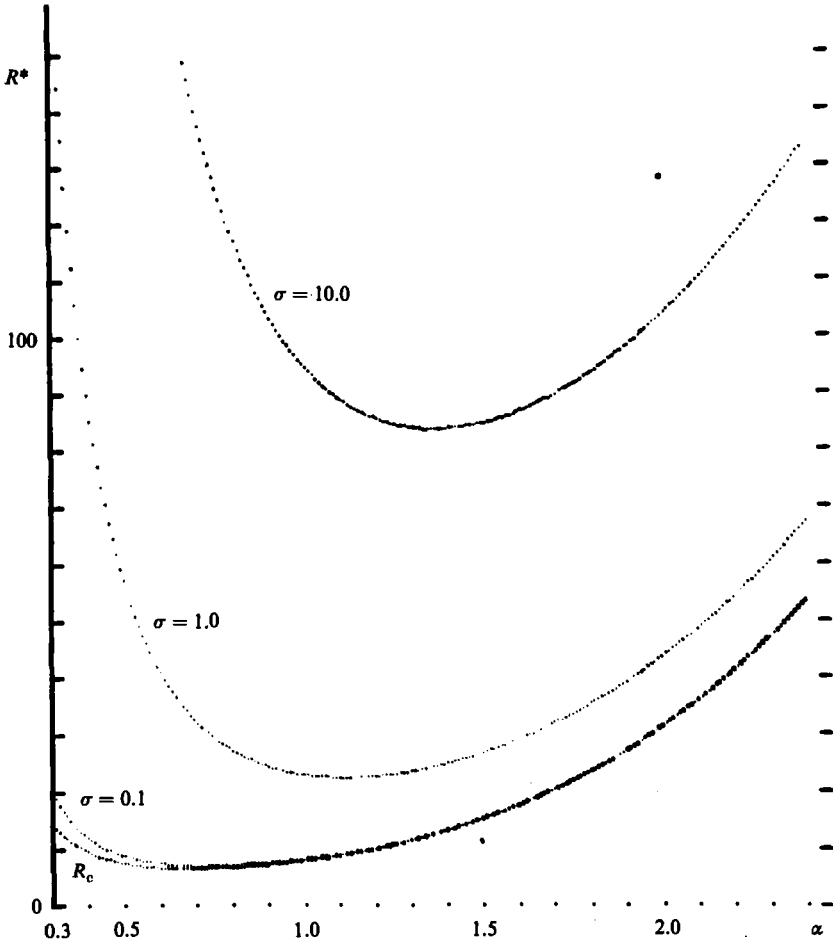
FIGURE 3. R^* *vs.* α for various σ.

The remaining two equations (8) and (10) can each then be solved for R in terms of A^2 and C^2; by eliminating R between them we obtain a relationship between A^2 and C^2 that can always be solved for A^2 in terms of C^2, namely

$$\left[\frac{3\alpha^2(4+\alpha^2)}{8\sigma^2} + \frac{3(1+\alpha^2)^2}{8\sigma} + \frac{(1+\alpha^2)^2}{8} + \left(\frac{27\alpha^2}{64\sigma^3} + \frac{3\alpha^2(3+\alpha^2)}{64\sigma^2} \right) C^2 \right] A^2$$

$$= R_2 - R_c - \frac{3}{8\sigma^2} [(1+\alpha^2)(3+\alpha^2) + \sigma(4+\alpha^2)^2] C^2. \quad (11)$$

This can be used to eliminate A^2 in one of the equations for R, thereby obtaining R in terms of C^2. A is likewise determined in terms of C^2, except for sign, by this relation, and then the above equations for B, D, E and F give the remaining components in terms of C and the sign of A. Because R is determined by C^2 and there are two independent ambiguous signs in going from C^2 to C and A, there are four critical points for each value of R that occurs. C^2 is limited to the range that makes the right-hand side of (11) positive, and it is easy to show that the corresponding range of R is from R_c to R_2. In figure 1, the four tilted-cell critical points are labelled

TC + +, TC + −, TC − +, TC − −. The first sign refers to the Lorenz branch, the second to the two possible angles of tilt of the cell.

An example of streamlines of these steady tilted cells is shown in figure 4 (*a*). The horizontal average of the horizontal velocity component $\bar{u}$ is non-zero. Yet it is clear from the streamlines in the figure that a fluid parcel in one cell remains forever in that cell. There is an Eulerian, but not a Lagrangian average $\bar{u}$.

Although *steady* convection with all cells tilted in one direction is not observed in laboratory fluid layers, it is observed in a Hele-Shaw cell. Although this flow, an example of which is seen in figure 4 (*b*), is governed by different equations it is interesting to see that some cellular convection actually does undergo this symmetry-breaking transition.

The steady tilted cells become unstable at $R = \tilde{R}$, where there is a supercritical Hopf bifurcation as a complex-conjugate pair of eigenvalues crosses the imaginary axis and acquires a positive real part. For $\sigma = 1$ and $\alpha = 1.2$, this occurs at $R = 38.802$. Table 1 and figure 2 (*a*) show critical values for other α and σ.

$R > \tilde{R}$

With the instability of the tilted cell at $\tilde{R}$ a stable limit cycle grows out of each of the four critical points TC + +, TC + −, TC − +, and TC − −. These are indicated schematically in figure 1. Solutions were obtained by numerically integrating (5)–(10) in time using a fourth-order Runge–Kutta method. Stable periodic solutions were found over much of the following ranges of R:

$$11.215 < R < 120 \quad \text{for } \sigma = 0.1,$$

$$38.802 < R < 140 \quad \text{for } \sigma = 1.0,$$

$$89.179 < R < 130 \quad \text{for } \sigma = 10.$$

We first describe the solutions found at R just greater than $\tilde{R}$. These are periodic with period determined very nearly by the imaginary part of the unstable eigenvalue. For an initial condition taken near TC + +, for example, the values of A, B, ..., F obtained at each time step were plotted on various projections. Some examples of plots of the orbit on an A–C projection will be shown. At R slightly in excess of $\tilde{R}$, this is a simple closed curve around TC + +. In figure 5, the curve labelled (1) is the projected orbit for $\sigma = 1.0$, $\alpha = 1.2$, $R = 38.9$; the curve labelled (2) is for $R = 42.5$. From the values of A, ..., F the temperature and stream function can be constructed. One example of the temperature field at times equally spaced within one period, is shown in figure 6. A hot plume or bubble is seen to form in the lower part of the region, rise and tilt from lower left to upper right. Later, a cold plume forms in the upper part, sinks and tilts from upper right to lower left. It also shows a leftward-propagating wave in the isotherms near the bottom of the layer and a rightward-propagating wave near the top of the layer. Similar orbits were found for $\sigma = 0.1$ and $\sigma = 10.0$, for R slightly in excess of $\tilde{R}$.

The periods of the stable limit cycles are plotted against R in figure 7 (*a*) for $\sigma = 0.1$, 7 (*b*) for $\sigma = 1.0$, and 7 (*c*) for $\sigma = 10$. With the exception of the five circled points in figure 7 (*c*) all other points represent stable periodic solutions; the many unstable ones that were computed have not been included on these plots.

These figures show narrow Rayleigh-number ranges in which the period increases rapidly with R. Figure 7 (*b*) for $\sigma = 1.0$, in particular, has several such 'spikes' separating broad ranges of nearly constant period. These spikes occur near $R = 44.5$, 51, 91, 95, 115. We will now describe the behaviour of the flow near these spikes.
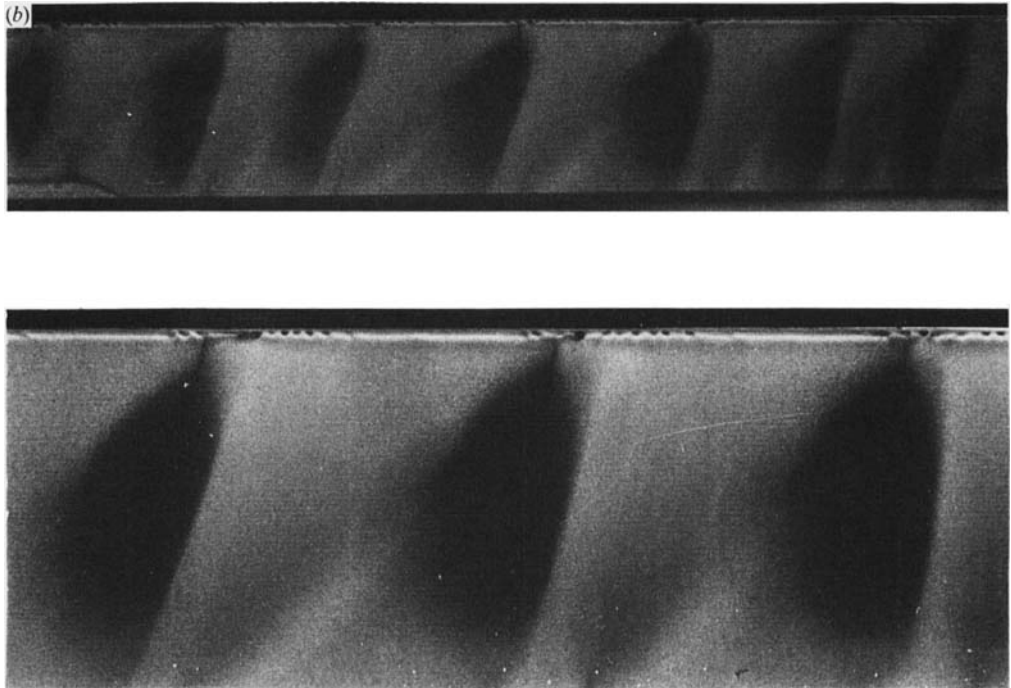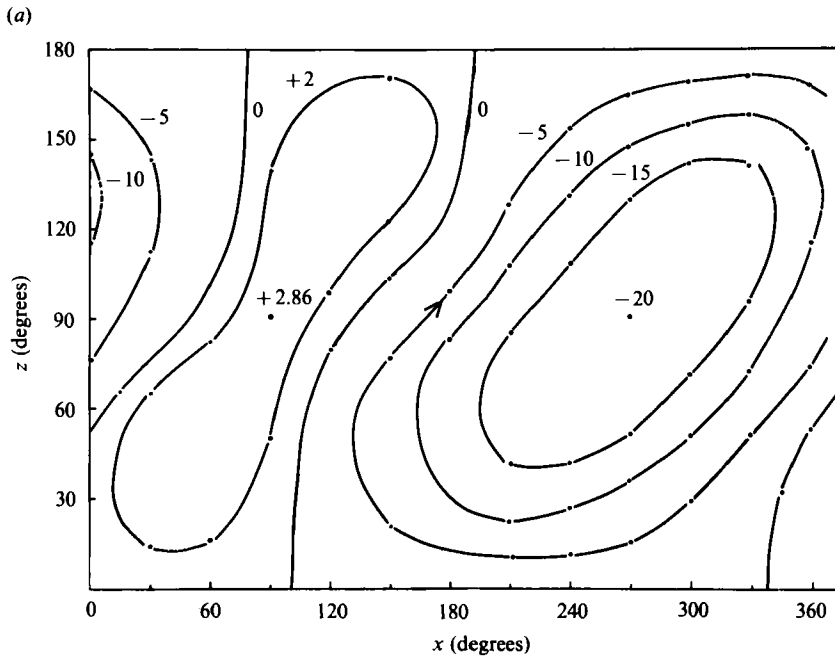
FIGURE 4. (a) Streamlines showing steady tilted cellular flow that occurs after the second bifurcation. $\sigma = 5.0$, $\alpha^2 = 0.5$, $R = 143$. (b) Steady tilted cellular flow in a Hele-Shaw cell, forced only by evaporative cooling of the top of the fluid, which was freon 113, 7 cm deep, 75 cm wide, 0.1 cm thick (in the direction normal to the page).
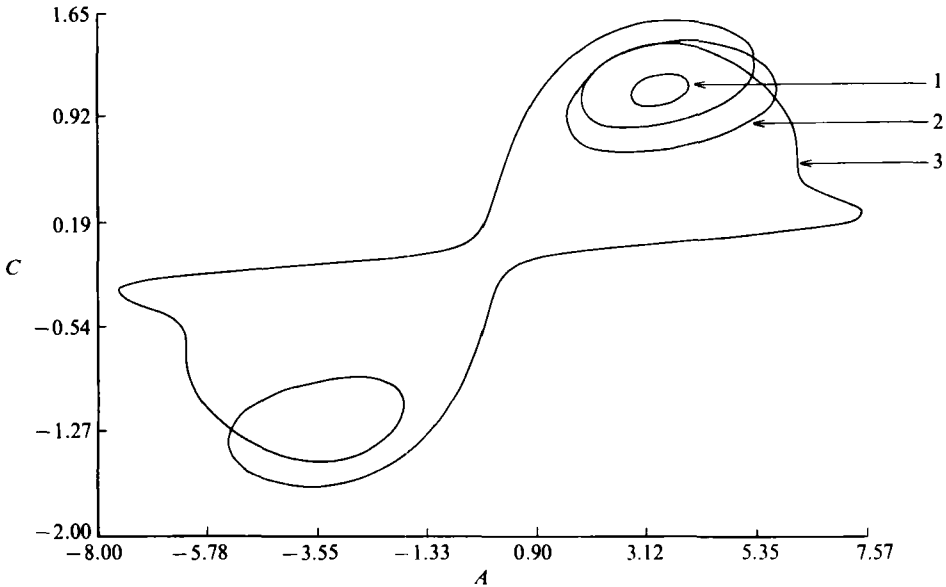
FIGURE 5. Projections of periodic orbits in phase space onto the (A, C)-plane. $\sigma = 1$, $\alpha = 1.2$; curve (1) $R = 38.9$; curve (2) $R = 42.5$; curve (3) $R = 44.601$.

$R > \tilde{R}, \sigma = 1.0$

Approaching $R = 44.5$ from lower values of R, the simple orbit described above undergoes period doubling. The doubled period is stable for a certain range of R until one eigenvalue of the Poincaré map becomes -1. Beyond this point period 4 is stable for a certain range of R until it also goes through a period-doubling bifurcation and period 8 becomes stable, and so on to period 2^n. Approaching $R = 44.5$ from higher values of R there is another period-doubling sequence for decreasing R. Between these two sequences is a range of R where the flow was chaotic and no stable periodic solutions were found.

At $R \approx 45$, as well as at $R \approx 44$, there was a strong dependence upon the initial condition and multiple stable solutions at the same value of R were found. The hysteresis curve for $R \approx 45$ is shown in figure 8. The arrows indicate that the solution at the value of R at the tip of the arrow was obtained using as the initial condition the solution for R at the tail end of the arrow.

We will show below that there is a pair of heteroclinic solution curves making a closed 'orbit' at $R \approx 44.5$, and that associated with this is a chaotic invariant set.

In the range $45 < R < 50$, stable periodic solutions were found whose (A, C)-projection is as shown in figure 5, curve (3). Instead of remaining near the critical point TC$+ +$, the orbit now comes near TC$- -$ as well as near $L+$, $L-$ and 0.

Behaviour similar to that at $R \approx 44.5$ is found near $R \approx 51$. In this case however, approaching $R = 51$ from below, the periodic solutions end with an eigenvalue of the Poincaré map of $+1.0$, the last periodic solution being at $R = 50.214$. Approaching from above, the eigenvalue passes through -1.0 and there is again a period-doubling sequence for decreasing R. The value of R, designated R_n, at which the period 2^n orbit has eigenvalue -1.000 ± 0.001 is shown in table 2. The orbit of period 2^n is stable from the point where it was formed (when the Poincaré map of the period 2^{n-1} orbit had eigenvalue -1) to the point where it has eigenvalue -1. However only the latter
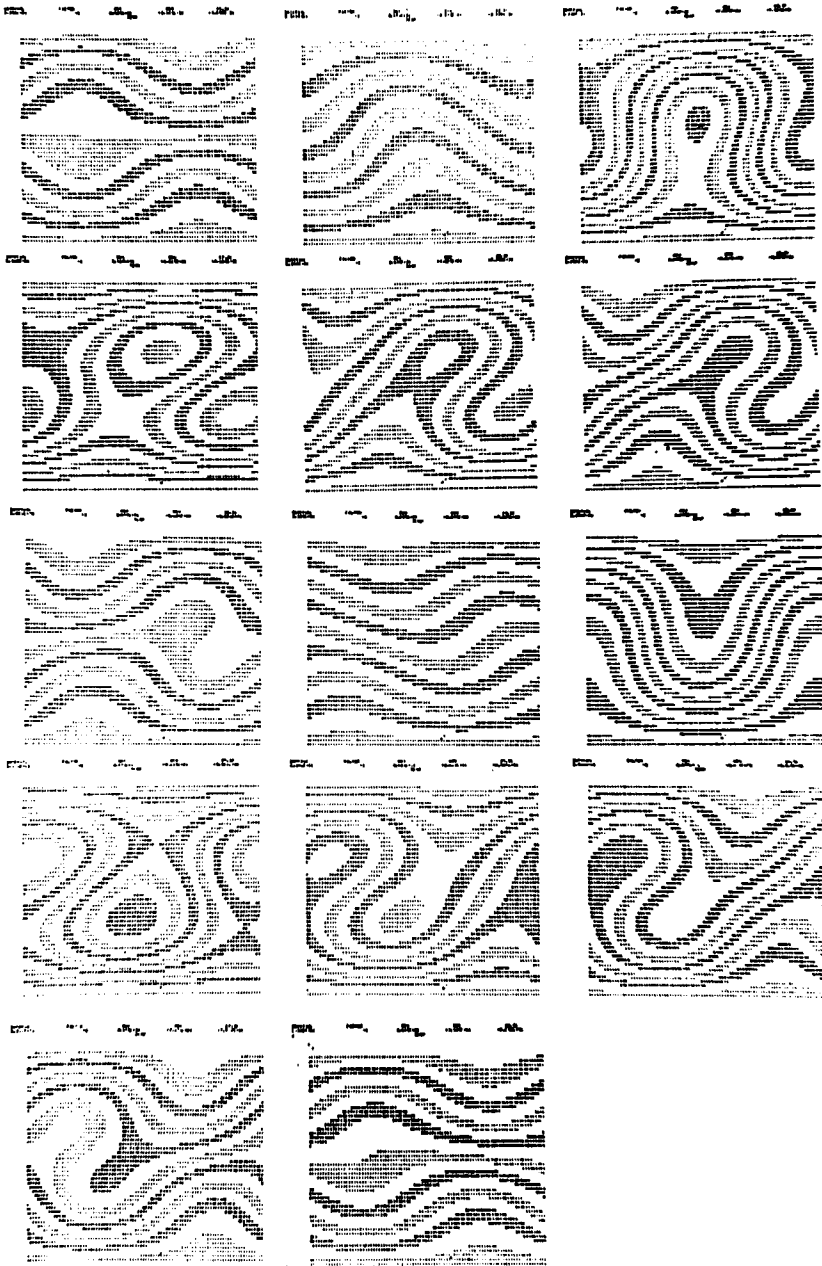
FIGURE 6. Temperature field at successive time intervals within one oscillation period. $\sigma = 1.0$, $\alpha = 1.2$, $R = 55$.

value, R_n, was used in calculating δ_n defined below. These multiple-period orbits were calculated by numerically constructing the Poincaré map and finding fixed points by using a secant method.

The ratio $\delta_n = (R_{n-1} - R_n)/(R_n - R_{n+1})$ took the following values:

$$\delta_1 = 4.603, \quad \delta_2 = 4.7169, \quad \delta_3 = 4.50, \quad \delta_4 = 4.88.$$
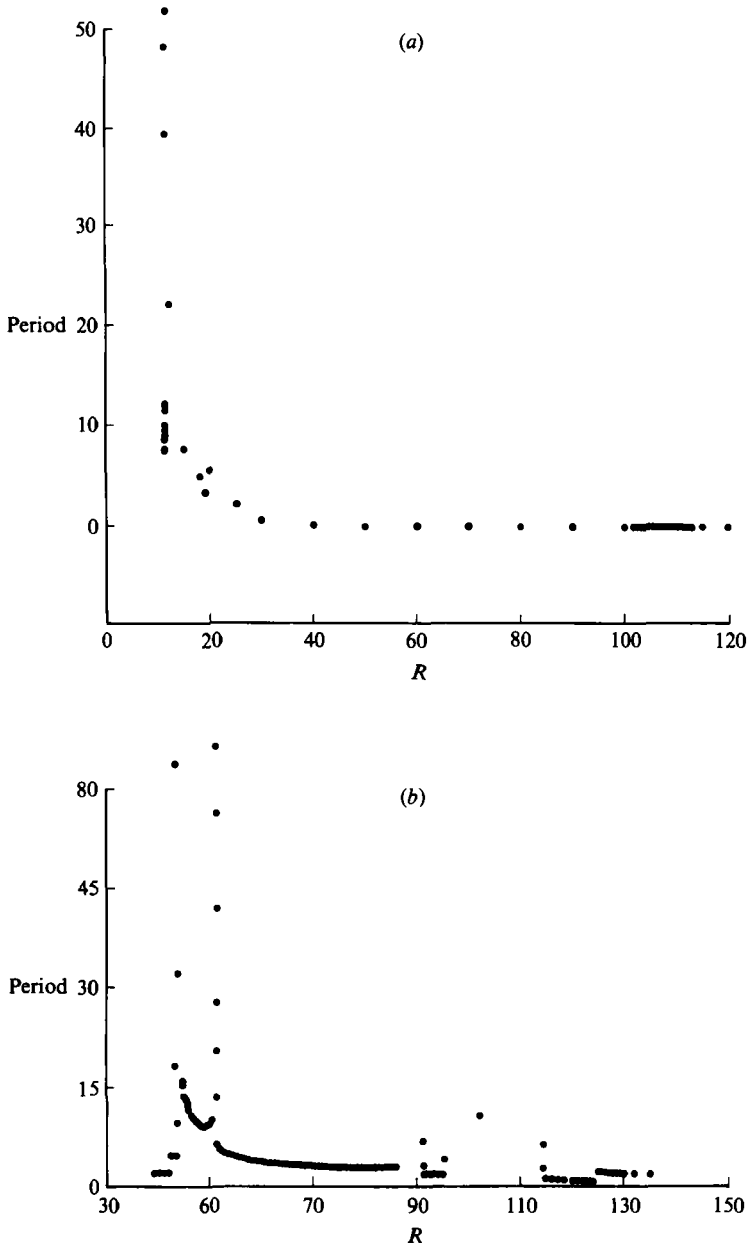
FIGURE 7 (a, b). For caption see facing page.

For a large class of one-dimensional maps the ratio δ_n approaches a universal constant $\delta_n = 4.662\ldots$ as $n \to \infty$ (Feigenbaum 1978). Although we have a five-dimensional section (usually made at $A = 0$), it probably closely approximates a one-dimensional map because while one eigenvalue of the Poincaré map is -1 (at the bifurcation point), the other four are typically 10^{-6}–10^{-8}. The ratios cited above are all near 4.66, but do not look particularly convergent. However, accurate determination of these ratios for large n requires a great deal of attention to numerical accuracy – even locating a fixed point is tricky, for at high n there are many
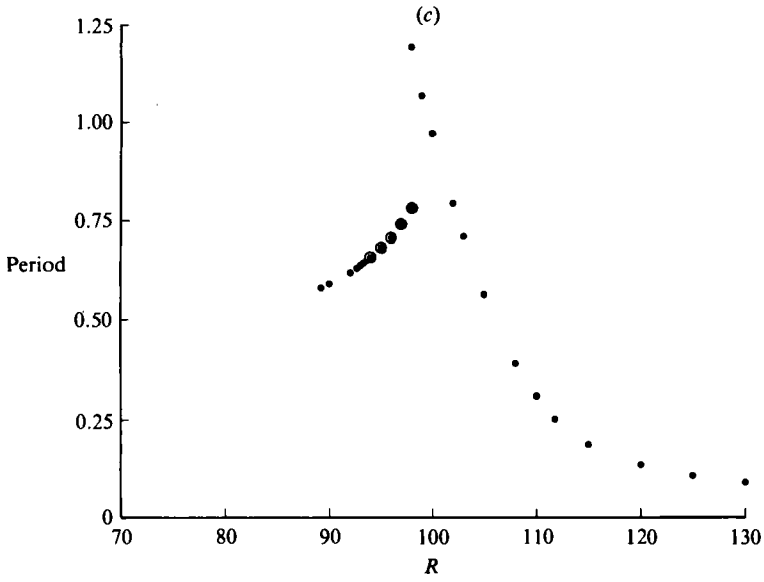
FIGURE 7. Period *vs.* Rayleigh number for (*a*) $\sigma = 0.1$, $\alpha = 1.2$; (*b*) $\sigma = 1.0$, $\alpha = 1.2$ (*c*) $\sigma = 10$, $\alpha = 1.2$.
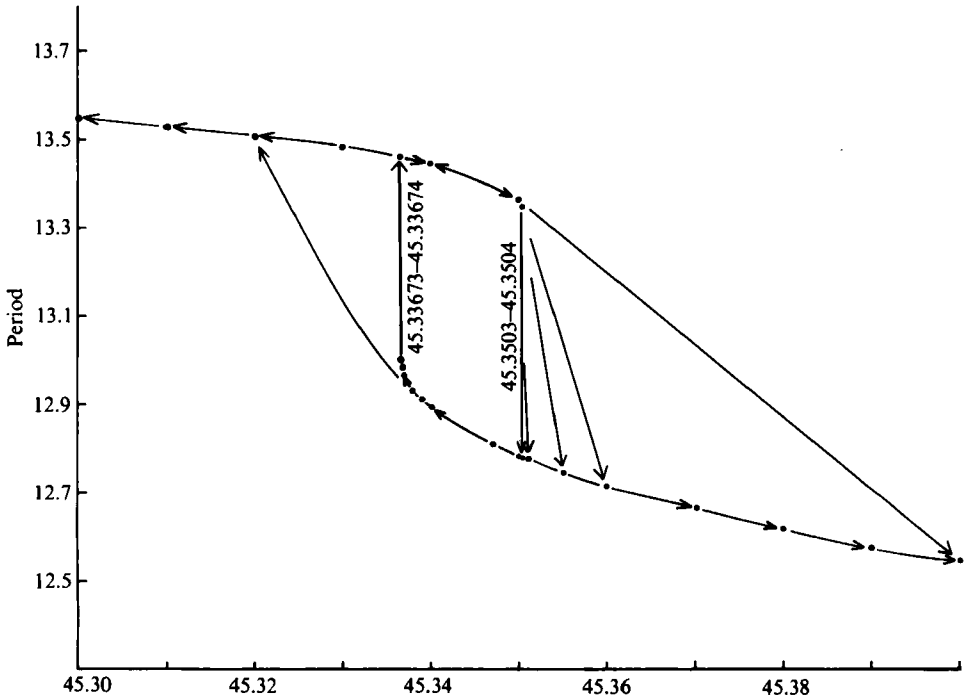

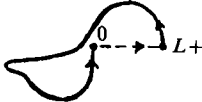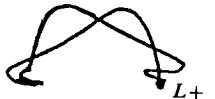FIGURE 8. Period *vs.* Rayleigh number for $\sigma = 1.0$, $\alpha = 1.2$, near Rayleigh number $= 45$.

R	Orbit Prandtl number $= 1$	Attracting chaos?
44.525 753 076 3		Yes
48.392 829 255		No
48.438 009 0		No
48.798 777 115		No
50.652 486 478		Yes
50.994 196 841 2		Yes
86.417 176 473 6		Yes
87.078 508 703 2 (Homoclinic orbit)		Yes
Or		

TABLE 2. (Continued on next page)

R	Orbit Prandtl number = 0.1	Attracting chaos?
11.29772	0 L+	Yes
13.12955	0 L+	
15.5734027778	0 L+	
18.1533617021	0 L+	
20.4931946437	0 L+	
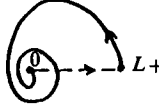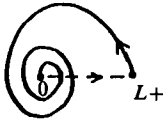
TABLE 2. Rayleigh number at the heteroclinic orbit pairs.

other fixed points close by, among which the secant method may jump around as R is varied in search of the bifurcation point. [The algorithm for finding fixed points is convergent at any fixed point, whether or not stable, provided that $+1$ is not an eigenvalue there and that one starts close enough.] On the whole this appears to be an 'ordinary' period-doubling sequence, apparently followed (as R decreases toward 51) by small regions of stable periodic orbits with periods of the form $(2k+1)\,2^n$ and ending with a period-3 orbit at about 51.193. This is a familiar pattern which has been carefully explored in various instances, and it did not seem necessary to refine the calculations enough to verify more convincingly the convergence of δ_n. It should perhaps be mentioned that although we used a 60-bit computer, the accuracy of the numerical integrations was not sufficient to ensure that the R_n are the true bifurcation points of the differential equation to as many decimal places as determined. But all integrations were done with the same algorithm and step size, so these numbers are probably correct for *some* differential equation closely approximating (5)–(10).

Between $R = 51.193$, where the period-3 orbit loses stability, and $R = 50.214$, where the simple periodic orbit ends with eigenvalue $+1$, we found mostly chaotic and very few periodic solutions. For example, at $R = 50.23$ the (A, C)-projection of an orbit obtained by forward integration for a considerable time is shown in figure $9\,(a)$. The power spectrum for this case (figure $9\,b$) shows a broad spectrum superimposed on the peaks corresponding to the period of simple orbits. The coordinate B
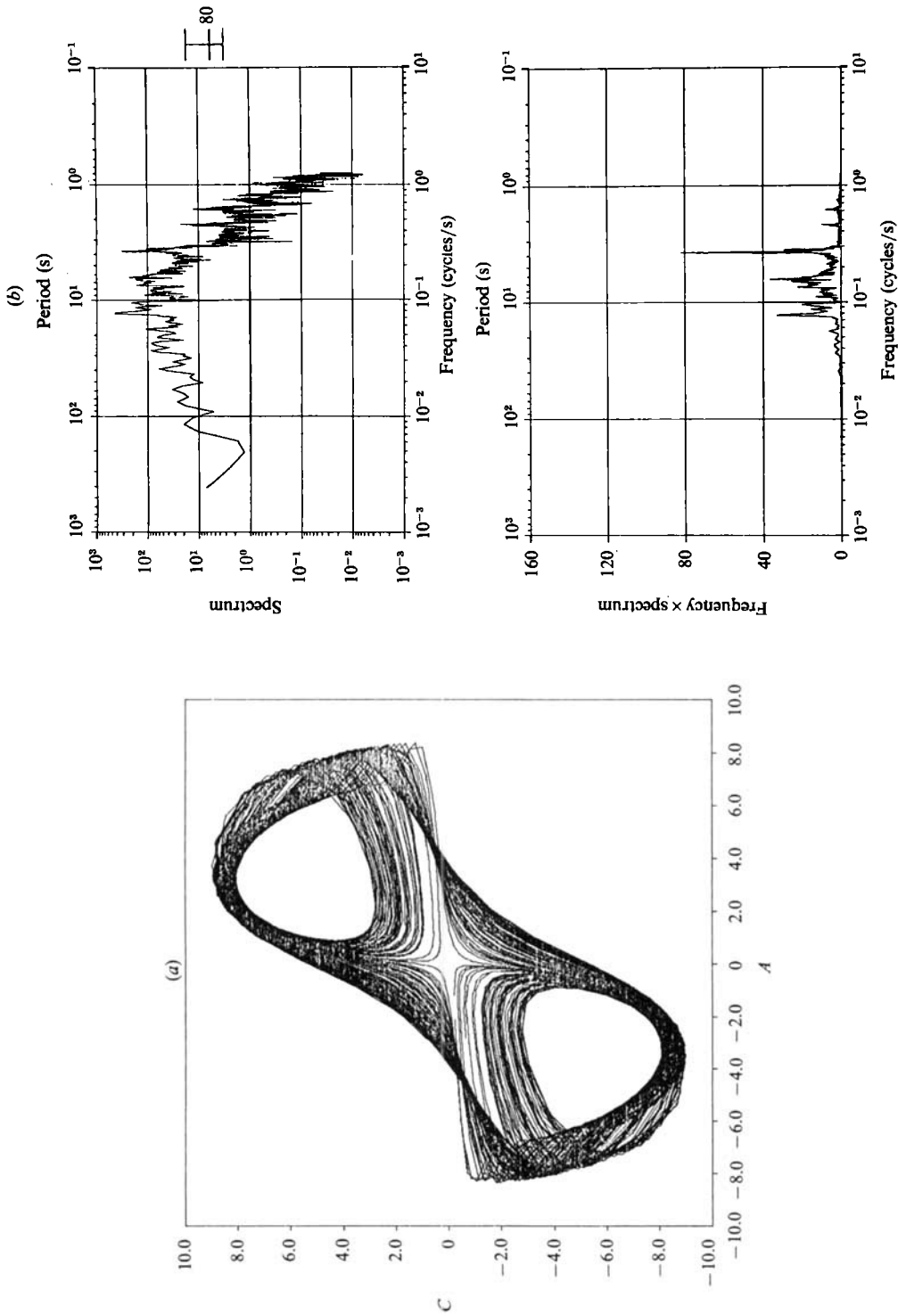
FIGURE 9. (*a*) (*A*, *C*)-projection at $R = 50.23$, $\sigma = 1.0$, $\alpha = 1.2$. (*b*) Spectrum *vs.* frequency for the same parameters as in figure 9(*a*).
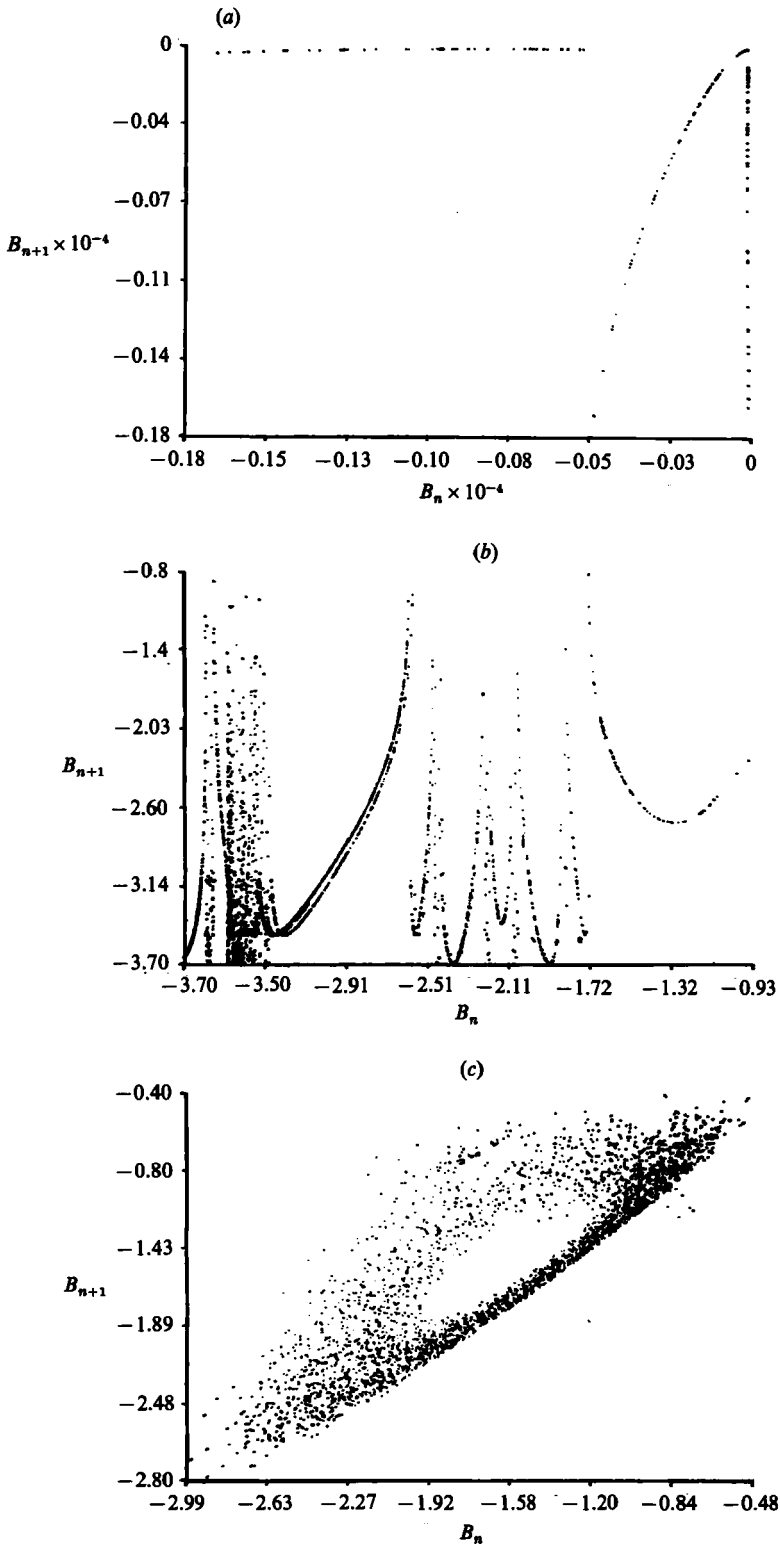
FIGURE 10. Map of successive returns (B_{n+1} *vs.* B_n) for (a) $\sigma = 0.1$, $R = 11.4$; (b) $\sigma = 1.0$, $R = 50.23$; (c) $\sigma = 10.0$, $R = 93.4$.

at successive returns (B_{n+1} *vs.* B_n) is plotted in figure 10(b). Resemblance, in parts of this figure, to a high-order one-dimensional map is noted, though it does not seem to be single-valued in terms of the coordinate B. If the intersection of the attractor on which this orbit (nearly) lies with the five-dimensional plane of section is indeed something like a curve, it is evidently a rather complicated one. (The successive-returns plot at $R = 44.55$ appears similar to figure 10a.)

As at $R \approx 44.5$, there is a pair of heteroclinic solution curves forming a closed 'orbit' at $R \approx 51$.

In the range $51.286 < R < 85.7$ simple periodic solutions are once more stable. The (A, C)-projection of the orbit in this range has once more changed shape; it no longer 'circles' TC+ + and TC− −, and as R is increased it also moves further away from the origin. At $R \approx 85.695$, these periodic orbits end with eigenvalue +1, and the range $85.695 < R < 91.2$ is full of chaotic flows. Once again, a heteroclinic orbit pair occurs at $R \approx 86.4$; there is also a homoclinic orbit from $L+$ to itself at $R \approx 87.1$.

There are further period-doubling sequences; at $R \approx 91.179$ there is period doubling for decreasing R. There are stable periodic orbits for $91.179 < R < 95.16$. At $R = 95.16$, there is period doubling for increasing R, then most flows are chaotic from 95.16 to 114.5. There is period doubling at 114.5 for R decreasing, and stable periodic orbits for $114.5 < R < 125$.

$R > \tilde{R}, \sigma = 0.1$

The periods of stable limit cycles *vs.* R are shown in figure 7(a). Rayleigh numbers for occurrences of heteroclinic orbits are summarized in table 2. (These are clearly not all possible heteroclinic orbits.) The behaviour at $\sigma = 0.1$, $\alpha = 1.2$ is similar to that at $\sigma = 1$, $\alpha = 1.2$. However, in this case, $\tilde{R} = 11.215$ is quickly followed by a heteroclinic orbit pair at $R = 11.2972$, and by many other such pairs soon thereafter. Some cases of period doubling were noted, but stable periodic orbits were generally difficult to find in the range $11.3 < R < 20$. Presumably behaviour similar to that for $\sigma = 1.0$ occurs but in a smaller range of R and it is harder to sort out, and bifurcation sequences are not shown in figure 7(a). The large periods near $R = 11.3$ are not multiples of simple periodic orbits but results of close approach to the origin. The plot of successive returns of B (B_{n+1} *vs.* B_n) at $R = 11.4$ is shown in figure 10(a).

$R > \tilde{R}, \sigma = 10$.

For $\sigma = 10$ the problem restricted to the Lorenz space (A, D, E) itself undergoes bifurcations. For $\alpha = 1.2$, the first homoclinic orbit through the origin occurs at $R \approx 103$ and a Hopf bifurcation occurs at $R \approx 200$. However, as seen from table 1, the instability of the tilted-cell critical point occurs below these values, at $\tilde{R} = 89.179$. The periods of the stable limit cycles are plotted against R in figure 7(c). As with $\sigma = 1.0$ and 0.1, the orbit in (A, C)-projection at R just in excess of $\tilde{R}$ is a simple closed curve near one of the tilted-cell critical points, say TC+ +. For these, the period is shown in the left-hand branch of figure 7(c). At $R \approx 93$ the Poincaré map of these periodic orbits has a complex-conjugate pair of eigenvalues crossing the unit circle. In the range $93 < R < 98$, we found chaotic solutions. A plot of successive return (B_{n+1} *vs.* B_n) in this range is shown in figure 10(c). For $R \geqslant 98$ there are stable periodic orbits that approach the neighbourhood of both TC+ +, and TC− +. These are stable up to $R = 130$ and are represented by the right-hand branch in figure 7(c).

2.2. *Mass, momentum and heat fluxes*

Chaotic aspects of the flow, and their relationship to the existence of heteroclinic orbits will be discussed below. We now turn to some model results which are related
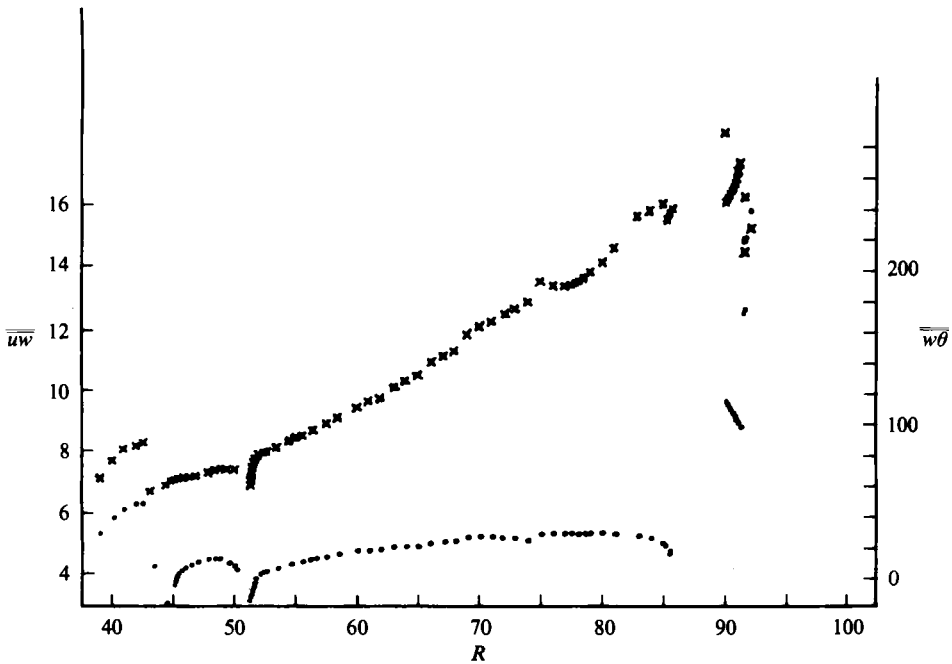
FIGURE 11. Vertical momentum flux $\overline{uw}$ (...) and vertical heat flux $\overline{w\Theta}$ vs. R (***).

to observable physical quantities such as the heat and momentum flux, and the Lagrangian transport of mass, all of which were observed in the laboratory experiments that motivated this model study. Although we do not expect quantitative agreement between results of this low-order model and the laboratory experiments, certain trends in the results suggest further experiments. For $\sigma = 1.0$, $\alpha = 1.2$, the convective heat flux $\overline{w\Theta}$ (the bars represent time- and horizontal-average) and the vertical transport of horizontal momentum $\overline{uw}$, evaluated at mid-depth, are plotted against R in figure 11. The momentum flux at mid-depth is $\overline{uw} = \alpha \overline{AC}$, the time-average of $\alpha \overline{AC}$. This is seen in figure 11 to be slowly varying, and remaining at approximately 5 for $45 < R < 85$, except near the heteroclinic points (where the system spends most of its time near the conduction state). However, for $R \geqslant 90$, the momentum flux very rapidly increases to values of around 15.

For a particle on the boundary ($z = 0$), the vertical velocity is zero and its position $G(t)$ relative to its position at $t = 0$ may be determined by integrating $\dot{x} = u(x(t), A(t), B(t), C(t))$. Examples of $G(t)$ vs. t for $\sigma = 1.0$ are seen in figure 12. For R just greater than $\tilde{R}$, the particle makes hesitating non-monotonic progress towards $x = -\infty$; as R is increased this becomes a more uniform drift. For $\sigma = 0.1$ and $R > \tilde{R}$ a particle on the boundary drifted smoothly toward $x = -\infty$, but for $\sigma = 10$, $R > \tilde{R}$, there was no net drift, only an oscillation in time with the particle remaining within one horizontal wavelength of its original position.

2.3. *Heteroclinic orbits and chaos*

Some years ago, Silnikov (1965) investigated the following situation. Suppose we have an autonomous system of differential equations in three dimensions which has a critical point with one positive real eigenvalue and two complex ones with negative real part. Thus the unstable manifold of this critical point is one-dimensional, and consists of two orbits going out along the unstable eigenvector in opposite directions, while its stable manifold is two-dimensional, being transverse to the unstable
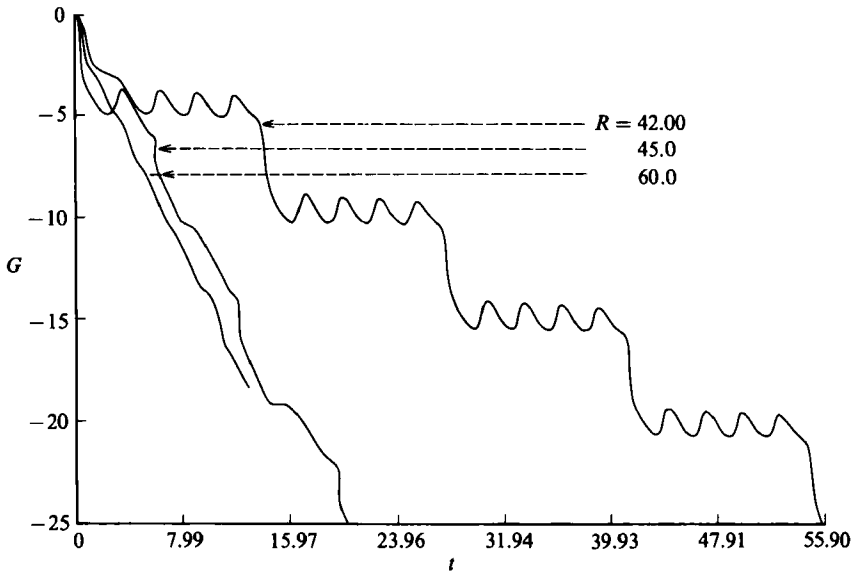
FIGURE 12. Horizontal coordinate G of a particle on the boundary, as it changes with time t.
$\sigma = 1.0$, $\alpha = 1.2$.

eigenvector at the critical point. Suppose further that one of the orbits making up the unstable manifold returns again, as $t \to +\infty$, to the critical point, forming a *homoclinic orbit*. This situation is of course most unlikely – even if the unstable manifold were to return to the neighbourhood of the critical point, there is no particular reason that it should be among the 'select few' orbits (all on a surface in 3 space) which form the stable manifold. On the other hand, if one is concerned not with a single system of differential equations but with a family of them depending on a parameter (like R in the model discussed above) it is no longer especially unlikely that a homoclinic orbit might occur at certain exceptional values of the parameter. [A homoclinic orbit for a single system of equations is structurally unstable – even if it happens, it can be destroyed by an arbitrarily small perturbation of the equations. But its occurrence for one among a one-parameter family of systems is not (with some mild transversality condition) – a small perturbation of the equations can be compensated for by a slight adjustment of the parameter.]

In this situation, Silnikov found that (with a certain mild transversality condition) provided the exponential growth rate of the unstable eigenvalue exceeded the exponential compression given by the magnitude of the real part of the complex eigenvalues then one could show the existence of infinitely many periodic orbits in every neighbourhood of the homoclinic one, and in fact of a whole chaotic set of orbits of the kind associated with a 'horseshoe map.' These include 'transition orbits' which approach different ones of the periodic orbits as $t \to +\infty$ and $-\infty$, as well as others which continually wander among neighbourhoods of many different periodic orbits and other irregular orbits – all this in every neighbourhood of the homoclinic orbit.

Now in the case of our six-dimensional model we do not have quite the situation considered by Silnikov, but there is a certain analogy. At some special values of R there are *heteroclinic* orbits going from the Lorenz critical point to the conduction one. The former has one unstable real eigenvalue and two stable complex ones,

these corresponding to a part of the stable manifold lying in the Lorenz space $B = C = F = 0$ (at least for Prandtl number = 1), and three other stable eigenvalues. The conduction critical point has an unstable real eigenvalue corresponding to an eigenvector in the Lorenz space, and five stable real ones – an 'ordinary' saddle point. There is a second heteroclinic orbit, lying in the Lorenz space, which connects the conduction state back to the Lorenz critical point. In general, it is even less likely that there should be a heteroclinic pair like this, making together a degenerate closed 'orbit', than that there should be a homoclinic orbit (usually one would have to adjust two parameters to make it happen). But in our case, because the Lorenz space is an invariant manifold containing the unstable manifold of the conduction critical point and because within this space the Lorenz critical point is completely stable, the return heteroclinic orbit *always* occurs (at least in the range of R of interest at $\sigma = 1$). Thus by adjustment of only one parameter (R) we can arrange for the heteroclinic pair.

Silnikov has also extended his results (see Silnikov 1970) to arbitrary dimension, and we have been able to modify his arguments to obtain a similar result to his if there is a heteroclinic pair joining a real saddle point with one unstable eigenvalue to a spiral saddle point with two stable complex eigenvalues (whose real part is numerically less than that of other stable eigenvalues) and one unstable eigenvalue. Here the condition on the relative magnitudes of compression and expansion is replaced by a somewhat more complicated condition involving these magnitudes at both critical points. In certain parameter ranges, our six-dimensional model is like this, but it has an additional feature which comes about because of the symmetry of the equations: when a heteroclinic orbit exists from $L+$ to 0, there is also another one from $L-$ to 0, and in fact both branches of the unstable manifolds of $L+$ go to 0 making four such heteroclinic orbits. Because of this there is a second chaos-producing mechanism somewhat analogous to that which produces the chaotic invariant set in the Lorenz model at high enough σ, and which is described for instance in Sparrow's book (1982, appendix D).

We have established a further modification of Silnikov's result, which applies to a somewhat generalized form of the kind of problem suggested by our six-dimensional model, involving both of these chaos-producing mechanisms. A description of this (without its proof) is deferred to the Appendix, since even this requires some distracting terminological preparations. Loosely speaking, the result is that in circumstances similar to those in the model, the occurrence of heteroclinic pairs implies the existence of a complicated (but qualitatively describable) invariant set of uncountably many orbits, each staying close to the system of heteroclinic orbits for all time.

The existence of a chaotic invariant set such as is given by results like Silnikov's unfortunately does not imply the existence of a chaotic *attractor*. But if one suspects that the latter occur only in a relatively small part of parameter space, it would seem that at least a good place to start looking would be near regions where chaotic sets – attracting or not – are present, for instance near the occurrence of heteroclinic pairs. In fact our numerical experiments with the six-dimensional model have indicated a close association of the double heteroclinic values with the range of R in which we have found what appear to be chaotic attractors. We would suggest the search for such heteroclinic pairs, which is a much easier numerical problem than a comprehensive search through parameter space, as a useful pointer toward chaotic attractors.

3. Conclusions

This model, although obtained by severe truncation of two-dimensional free-boundary convection, still has some qualitative features resembling the laboratory observations that motivated this study, namely the spontaneous change of symmetry that leads to the large-scale flow. After the third bifurcation of the model, one also sees features such as transient tilted plumes and horizontal Lagrangian transport, reminiscent of the laboratory observations.

For fairly general autonomous systems, we have shown that the occurrence of heteroclinic orbit pairs is associated with chaotic invariant sets. This has helped to clarify the occurrence of chaos in the six-dimensional model, and may be of use similarly in more general models including the Boussinesq equations. We do suggest that the Boussinesq equations may have something like this heteroclinic chaos, but do not wish to identify that with the observed turbulence at high Rayleigh numbers.

Appendix

The modification of Silnikov's result alluded to above deals with a system $x' = F(x)$ of $n^* \geqq 3$ differential equations subject to four hypotheses, H1–H4. The most significant of these, H1 and H2, are described below. The other two are rather technical 'transversality' hypotheses which are nearly always satisfied but are needed for completeness to exclude certain exceptional cases. Unfortunately, merely the statement of these hypotheses (especially H3) requires a somewhat lengthy description of the technical aspects of the proof. H4 is given below also (but without much explanation), since some of the background to it is needed to state the final result. H3 is not needed for this – only for the proof – and its description is omitted. The details of this and of the proof will probably be published elsewhere; they are also in an extended version of this Appendix which is available from the authors. The description of the main hypotheses follows, and the result, called 'Theorem A', is given at the end. Some necessary terminology and notation is introduced in the course of the description.

We use the letters s and σ to stand for signs, $+$ or $-$, and the letter S for a pair of signs, an 'upper' one S^* and a 'lower' one S_*. We shall for instance write L_s for one of a pair of critical points $L+$ and $L-$, and H_S for one of four heteroclinic orbits H_+^+, H_+^-, H_-^+ and H_-^-. The first two hypotheses about the system $x' = F(x)$ are:

H1. There are three critical points, 0, $L+$ and $L-$, with the properties:
   (a) The linearization at 0 has one simple positive eigenvalue λ_0, one negative one $-\mu_0$, and all others have real parts $< -\mu_0$.
   (b) The linearization at L_s has one simple positive eigenvalue λ_s, one conjugate pair of simple complex eigenvalues $-\mu_s \pm i\omega_s$ with $\mu_s > 0$ (and $\omega_s > 0$), and all others have real parts $< -\mu_s$.
   (c) There is a number $\rho > 1$ such that $(\lambda_0 \lambda_s)/(\mu_0 \mu_s) > \rho$ for both choices of s.

H2. There are six heteroclinic orbits, H_s from 0 to L_s and H_S from L_{S_*} to 0. (The H_s form the two branches of the unstable manifold of 0, while the H_S, for fixed S_*, form the two branches of the unstable manifold of L_{S_*}.) These leave their initial points tangent to the unstable eigenvectors there; we assume also that they approach

their terminal points tangent to the *least* stable eigenvector there, or to the plane of its real and imaginary parts if it is complex.

These are clearly motivated by the situation in our idealized model, but there is no restriction to six dimensions, nor has any analogue of the symmetry properties of the model been hypothesized, since what is really needed in our proof is the simultaneous occurrence of six heteroclinic orbits. However this is so unlikely to happen in general that probably the result is actually of interest only when special circumstances, like symmetry and the invariance of the Lorenz manifold in the model, make the occurrence of one heteroclinic orbit automatically produce others. Arbitrariness of the dimension n^* is perhaps of more interest. Although we assume it to be finite, its essential irrelevance suggests that similar results can be expected if heteroclinic orbits can be found in similar problems of infinite dimension, like the real Boussinesq equations. Good numerical evidence for something of this sort (in a somewhat different context) has recently been given in Moore *et al.* (1983).

The geometrical structure made of the three critical points and the six heteroclinic orbits is now surrounded by an 'extended neighbourhood' N made of small 'balls' about the critical points, connected by thin 'tubes' about the heteroclinic orbits. Although most solutions of the differential equations whose orbits intersect N leave it for large enough $|t|$, Theorem A asserts the existence of many which stay in N for all t. The qualitative description of these is made by associating them with certain sequences of 'symbols' $\{\Sigma_k: -\infty < k < \infty\}$, in which each Σ_k is a quadruplet of signs and an integer: $\Sigma_k = (S_k, s_k, \sigma_k, n_k)$. Not all such sequences are relevant here; to describe those which are we need a little more terminology.

The heteroclinic orbit H_S goes from L_{S_*} to 0, and is the orbit of a particular solution x_S of the system. (For each S this solution is unique up to a translation in t.) We may choose this solution so that $x_S' \sim S^* \exp(\lambda_{S_*} t) e_{S_*}$ as $t \to -\infty$, where e_{S_*} is a (real) eigenvector of the linearization at L_{S_*} corresponding to the eigenvalue λ_{S_*}. As $t \to +\infty$ this solution approaches 0, and according to hypothesis H2 does so tangent to an eigenvector e_1 corresponding to the eigenvalue $-\mu_0$ of the linearization at 0. Thus we have $x_S' \sim -K_S S^* \exp(-\mu_0 t) e_1$ for $t \to +\infty$, the (non-zero) constant K_S being thereby defined.

Similarly we may select solutions x_s whose orbits are the H_s. Now linearize the system about the solutions x_s, getting $\xi' = M_s(t)\xi$, say, where $M_s = F_x(x_s(t))$. Since $x_s \to 0$ for $t \to -\infty$, $M_s(t)$ approaches (exponentially) the matrix of the linearization at 0, as $t \to -\infty$. (Likewise it approaches the matrix of the linearization at L_s as $t \to +\infty$.) We may thus choose a basis for the solutions of $\xi' = M_s \xi$ which has as first element a solution $\phi_{s1} \sim s \exp(-\mu_0 t) e_1$ as $t \to -\infty$ and has its other elements asymptotically orthogonal to l_1, the left eigenvector of the linearization at 0 corresponding to the eigenvalue $-\mu_0$, as $t \to -\infty$. Alternatively we may choose a basis which has as first element a solution $\psi_{s1} \sim \exp(\lambda_s t) e_s$ as $t \to +\infty$, where e_s is the eigenvector of the linearization at L_s corresponding to eigenvalue λ_s, and the other elements are asymptotically orthogonal to the corresponding left eigenvector l_s. The solution ϕ_{s1} is some linear combination of the elements of this second basis, and we shall write η_{s1} for the coefficient of ψ_{s1} in this. It is possible that η_{s1} is zero, but in general this is not the case; one of the transversality hypotheses is:

H4. $\eta_{s1} \neq 0$.

Now we call a sequence of symbols $\{\Sigma_k = (S_k, s_k, \sigma_k, n_k)\}$ *admissible* if

$$(S_{k+1})_* = s_k, \quad (S_{k+1})^* = S_k^* \operatorname{sgn}(K_S \eta_{s1}), \quad n_{k+1} > n_k/\rho + n_0,$$

where $\rho > 1$ is the number mentioned in H1(c) and n_0 is some fixed integer. There is obviously an uncountable infinity of such admissible sequences – for instance if $\rho = 10/9$ and $n_0 = 9$ each of the n_k can be chosen as 100 or 101, arbitrarily, and the last condition will always be satisfied. Since there are four signs and only two sign conditions, at each stage there are four admissible sign choices. Even if a sign sequence is fixed in advance, we still have as many of these (100 101) sequences as there are real numbers.

THEOREM A. *For an autonomous system of $n^* \geq 3$ differential equations satisfying the hypotheses H1–H4 and for any extended neighbourhood N of its critical points and heteroclinic orbits there is an n_0 such that to every admissible symbol sequence there corresponds an orbit which lies in N for all t. Symbol sequences which are not translates of each other correspond to different orbits.*

These orbits may be thought of as consisting of a succession of 'excursions' out from the neighbourhood of 0 to a neighbourhood of L_s along a path close to H_s, returning close to H_S. The symbol sequence gives a qualitative description of the orbit, the signs describing the switching between different excursion paths, and the integers n_k approximately measuring the lengths of time spent in the neighbourhoods of the critical points L_s.

One of the referees has called to our attention a recent paper, Tresser (1984). This interesting article gives a presentation and some generalization of Silnikov's theorems, and discusses some results on heteroclinic loops closely related to the one given here.

REFERENCES

BUSSE, F. H. & WHITEHEAD, J. A. 1971 Instabilities of convection rolls in a high Prandtl number fluid. *J. Fluid Mech.* **47**, 305–320.

CODDINGTON, E. A. & LEVINSON, N. 1955 *Theory of Ordinary Differential Equations.* McGraw-Hill.

CURRY, J. H. 1978 A generalized Lorenz System. *Communs Math. Phys.* **60**, 193–204.

FEIGENBAUM, M. J. 1978 Quantitative universality for a class of non-linear transformations. *J. Stat. Phys.* **19**, 25–52.

KRISHNAMURTI, R. 1970a On the transition to turbulent convection. Part 1. The transition from two- to three-dimensional flow. *J. Fluid Mech.* **42**, 295–307.

KRISHNAMURTI, R. 1970b On the transition to turbulent convection. Part 2. The transition to time-dependent flow. *J. Fluid Mech.* **42**, 309–320.

KRISHNAMURTI, R. & HOWARD, L. N. 1981 Large-scale flow generation in turbulent convection. *Proc. Nat. Acad. Sci.* **78**, 1981–1985.

LORENZ, E. N. 1963 Deterministic nonperiodic flow. *J. Atmos. Sci.* **20**, 130–141.

MALKUS, W. V. R. 1954 Discrete transitions in turbulent convection. *Proc. R. Soc. Lond.* A **225**, 185–195.

MOORE, D. R., TOOMRE, J., KNOBLOCH, E. & WEISS, N. O. 1983 Period doubling and chaos in partial differential equations for thermosolutal convection. *Nature* **303**, 663–667.

SILNIKOV, L. P. 1965 A case of the existence of a denumerable set of periodic motions. *Dokl. Akad. Nauk SSSR* **160**, 558–561 (*Sov. Math. Dokl.* **6**, 163–166).

SILNIKOV, L. P. 1970 A contribution to the problem of the structure of an extended neighbourhood of a rough equilibrium state of saddle-focus type. *Mat. Sbornik* **81**, 123 (*Math. USSR Sbornik* **10**, 91–102).

SPARROW, C. 1982 *The Lorenz Equations: Bifurcations, Chaos, and Strange Attractors.* Springer.

TRESSER, C. 1984 About some theorems by L. P. Silnikov. *Ann. Inst. Henri Poincaré* **40**, 441–461.

WILLIS, G. E. & DEARDORFF, J. W. 1967a Development of short-period temperature fluctuations in thermal convection. *Phys. Fluids* **10**, 931–937.

WILLIS, G. E. & DEARDORFF, J. W. 1967b Confirmation and renumbering of the discrete heat flux transitions of Malkus. *Phys. Fluids* **10**, 1861–1866.